Proceedings of the ASME 2018 37th International Conference on Ocean, Offshore and Arctic Engineering
OMAE2018
June 17-22, 2018, Madrid, Spain

OMAE2018-77826

CALIBRATION OF HYDRODYNAMIC COEFFICIENTS FOR A SEMI-SUBMERSIBLE 10 MW WIND TURBINE

Marit I. Kvittem *, Petter Andreas Berthelsen, Lene Eliassen, Maxime Thys

SINTEF Ocean
P.O. Box 4762 Torgard,
NO-7465 Trondheim, Norway

ABSTRACT

Hydrodynamic model tests and numerical simulations may be combined in a complementary manner during the design and qualification of new offshore structures. In the EU H2020 project LIFES50+ (lifes50plus.eu), a model test campaign of floating offshore wind turbines using Real-Time Hybrid Model (ReaTHM) testing techniques was carried out at SINTEF Ocean in fall 2017. The present paper focuses on the process of calibrating a numerical model to the experimental results. The concepts tested in the experimental campaign was a 1:36 scale model of the public version of the 10MW OO-Star Wind Floater semi-submersible offshore wind turbine.

A time-domain numerical model was developed based on the as-built scale model. The hull was considered as rigid, while bar elements were used to model the mooring system and tower in a coupled finite element approach. First-order frequency-dependent added mass, potential damping, and excitation forces/moments were evaluated across a range of frequencies using a panel method. Distributed viscous forces on the hull and mooring lines were added to the numerical model according to Morison's equation. Potential difference-frequency excitation forces were also included by applying Newman's approximation.

The quasi static properties of the mooring system were assessed by comparing the restoring force and maximum line tension with the pull-out test. Drag coefficients for the line segments were estimated by imposing the measured fairlead motion from model tests as forced displacement and comparing the calculated and measured dynamic line tension.

The linear and viscous damping coefficients were first estimated based on the decay tests, and the tuned damping coefficients were compared to initial guesses based on the Reynolds and Keulegan-Carpenter number at model scale. The results were then applied in the numerical model, and simulations in extreme irregular waves were compared to the experiments. It was found that second order drift forces proved to be significant, particularly for the severe irregular seastate. These could not be modelled correctly applying the potential drift forces together with quadratic damping matrix tuned to the free decay test. And the model with viscous drag coefficients tuned to decay tests also underestimated the slow drift motions. Thus, new viscous drag coefficients were determined to match the low frequency platform response.

To inverstigate the performance of the tuned model, comparisons were made for a moderate seastate and for a simulation with both waves and wind on an operating turbine. In the end, possible further improvements to the modelling were suggested.

INTRODUCTION

Model testing through physical experiments is an important part of validating numerical codes for response analysis of floating wind turbines. Benchmarking of different codes has been undertaken in the code-to-code comparisons in the IEA Task 23

*Corresponding author. Email: marit.kvittem@sintef.no.

(OC3) and Task 30 (OC4), and given valuable understanding of the implications of various modelling strategies. The most recent stage of the IEA task (Task 30 OC5) included validation of numerical codes against experiments, and one takeaway was that most codes underestimated the below wave frequency excitation force (see Robertson et. al. [1]). Berthelsen et. al. [2] focused in particular on calibration of the numerical model against experiments, to match the low frequency wave excitation. They propose a method to tune the viscous drag coefficients in the Morison formulation, and found good agreement with model tests on a slender braceless semi-subemersible.

A similar exercise to the one carried out by Berthelsen et. al. [2] is described in this paper. A numerical model was built in SINTEF Ocean numerical simulation workbench SIMA to replicate an Ocean Basin model test of a 10 MW semi-submersible wind turbine, and the viscous drag coefficients were tuned to match the platform response seen in the model tests. The dimensions of the semi-submersible in the study described herein are larger, less slender, than the study by Berthelsen, and thus it is expected that viscous effects may be less important.

Calibration of low frequency hydrodynamic loads in tests with floating wind turbines is known to be a challenge since the turbine loads also have a significant contribution to the low frequency loads on the platform. The model test used a real-time hybrid testing approach to model the loads from the turbine on the platform, which allows for isolating the response to hydrodynamic loads. This makes them easier to assess.

All the model specifications given in this paper are in full scale.

MODEL TEST DESCRIPTION

A model test campaign was carried out in the Sintef Ocean in November 2017, as part of the LIFES50+ project. The test model was a 1:36 scale model of a braceless, three-column semi-submersible designed to support a 10 MW turbine.

The turbine in the experiments was modelled using Real-Time Hybrid Model testing (ReaTHM® testing), where the rotor loads were applied at the top of the tower using six actuators positioned around the basin and connected to the model by thin lines. The rotor loads are computed in real-time based on the platform motions. A more thorough description of the system can be found in [3]. Similar systems were described by Sauder et. al. [4] and Bachynski et. al. [5].

Hull, tower and RNA

The model used for the case study is of the OO-Star Wind Floater [6] supporting the DTU 10MW reference wind turbine [7]. The main characteristics of the full model are shown in Tab. 1, and more detailed specifications can be found in [6]. The model was made with a stiff floater and a stiff tower with a flexible spring connecting the floater and the tower. The spring was designed to match the first tower natural frequency of the OO-Star Wind Floater, which has a fully flexible tower.

TABLE 1: FULL-SCALE CHARACTERISTICS OF THE MODEL.

Characteristic	Value	Unit
Mass	23 640	t
z_{COG}	-6.975	m
Inertia about origin x/y	28 460	kt m^2
Inertia about origin z	15 650	kt m^2
Draught	22	m
Diameter outer columns in WL	13.4	m
Outer column height	31.5	m
Diameter central column in WL	13.1	m
Central column height	33	m
Pontoon height (tapered)	6.5-7	m
Pontoon width (tapered, without girder)	16-17	m
Heave plate diameter	22.8	m
c/c central to outer column	37	m
Pontoon girder width	0.5	m

Mooring system

The mooring system consists of three catenary lines, one line attached to fairlead at the top of each column. Anchor and fairlead positions with the platform at rest are given in Tab. 2. Each mooring line consists of two sections of chain, attached with a spring. At the connection point between the upper chain segment and the spring, a clump weight is attached. Mooring line characteristics are listed in Tab. 3. The clump weight is listed here with length, but this is just for calculation of the integrated drag force, not part of the total length of the mooring line.

Test program

In the experiment, decay tests were carried out to determine natural frequencies and damping level in six degrees of floater motion. The decay tests were carried out with and without mooring and with and without the ReaTHM system lines attached,

TABLE 2: FARILEAD BODY COORDINATES AND ANCHOR GLOBAL COORDINATES.

	Fairleads		Anchors	
	z=9.5 m		z=-130 m	
Line no.	x (m)	y (m)	x (m)	y (m)
1	-44.0	0.0	-691.0	0.0
2	22.0	-38.105	345.5	-598.42
3	22.0	38.105	345.5	598.42

TABLE 3: MOORING LINE CHARACTERISTICS.

Segment	Length (m)	Diameter (m)	Submerged weight (kN/m)
Top chain	118.0	0.148	3.202
Clump weight	3.78	1.578	153.838
Spring	10.8		1.289
Bottom chain	572.4	0.148	3.123

and in different constant wind speeds. In addition, a hammer test was performed to verify the first eigenfrequency of the tower in fore-aft bending. Tests were run with irregular waves, irregular wind and combined irregular wind and waves. The wave spectrum used in the ocean basin was Pierson Moscowitz, and the wind spectrum used to generate the turbine loads was Kaimal. A list of the cases used for the current study are shown in Tab. 4.

NUMERICAL MODEL

A time-domain numerical model was developed based on the as-built scale model. The hull was considered as rigid, while bar elements were used to model the mooring system, and beam elements were used for the tower in a coupled finite element approach.

Coordinate system

The coordinate system used as reference in this paper is shown in Fig. 1.

TABLE 4: SELECTED CASES FROM THE TEST PROGRAM.

Test no.	Decription
2010/2021/2031/2040	Pullout tests
3110/3131/3151/3161	Decay tests
6250/6410	Irregular waves (no wind) (Hs=10.9m Tp=15s/ Hs=5.5m Tp=9s)
6231	Irregular waves with turbulent wind (Hs=10.9m Tp=15s U=18 m/s I=8.7%)

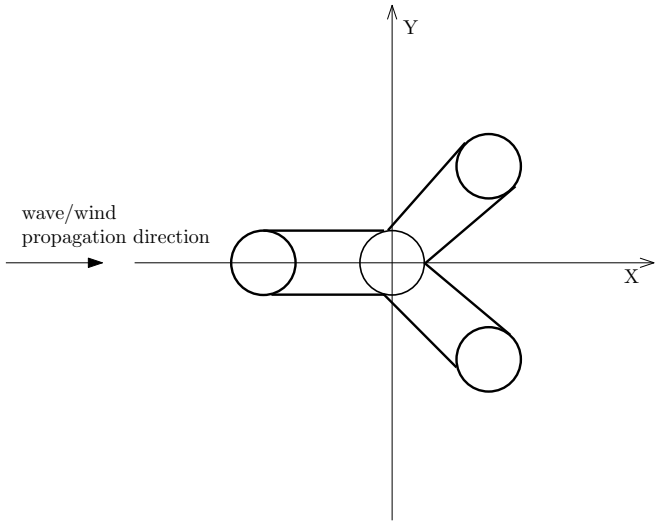

FIGURE 1: COORDINATE SYSTEM. Z IS ZERO IN MWL AND POSITIVE UPWARDS.

Hull, tower and RNA

The numerical model was built by applying a rigid body for the floater, flexible beam elements for the tower and flexible bar elements for the mooring lines. The tower was modeled by stiff beam elements, with a mass distribution as in the specification for the prototype.

The rotor-nacelle-assembly (RNA) was modelled as body with mass and inertia connected to the top of the tower. The RNA mass and centre of gravity (COG) were adjusted to match the overall mass, COG and inertia for the tower and RNA as measured in the scale model.

First-order frequency-dependent added mass, potential damping, and excitation forces/moments as a function of wave

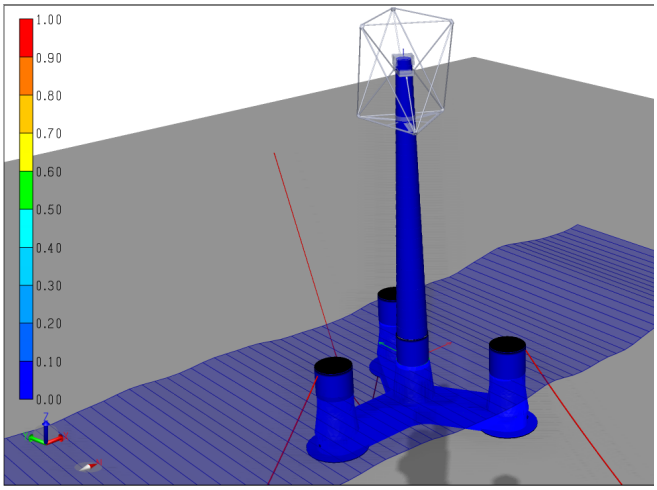

FIGURE 2: GRAPHICAL REPRESENTATION OF THE NUMERICAL MODEL IN SIMA. THE TURBINE WAS REPRESENTED BY A MASS MODEL AND TOWER TOP FORCES, AND IS HERE REPRESENTED BY A FRAME RESEMBLING THE MODEL TEST FRAME .

frequency were evaluated using a panel method model in WAMIT. Simplified potential difference-frequency excitation forces were also included in model using slow drift forces from the WAMIT analysis (Newman's approximation).

Distributed viscous forces on the hull and mooring lines were added to the numerical model according to Morison's equation. The width and height of the pontoons are slightly tapered, but for the viscous forces, constant dimensions (7 m heigh and 16 m width) are assumed. It was also assumed that the viscous drag elements on the pontoons extend from the centre of the central column to the centre of the outer columns. For the columns, viscous elements are applied from 11 m above MWL to the top of the pontoon (15 m below MWL). The heave plates stretch from 22 m below MWL and 0.5 m upwards.

The mooring system was modelled by bar elements, with different elements for the chain segments and the springs. The chain sections were given linear stiffness properties, whereas the spring stiffness was described by a bilinear force-displacement relationship. The clump weights were attached at the top of the lower chain segment.

Figure 2 shows a snapshot of the numerical model in SIMA.

CALIBRATION OF THE NUMERICAL MODEL

First, the mooring system in numerical model was verified by comparing the quasi-static and dynamic response to the measured line tension. Next, the free oscillation periods and damping of the system was compared to experimental decay tests, and the necessary calibration was performed to match the model test, as described below. Then, the horizontal drag coefficients were calibrated to match the response in irregular waves. The drag coefficients referenced in this paper, are defined by the non-dimensional parameter C_d in the drag term in a Morison type wave force expression, defined by Eq. 1.

$$dF_d = \frac{1}{2}\rho C_d A|u-\dot{x}|\,(u-\dot{x}) \tag{1}$$

where dF_d is the quadratic drag force acting on a strip of a submerged section, ρ is seawater density, A is the reference cross section area, u is the water particle velocity and $\dot{x}$ is the strip velocity in the direction of the water particle velocity. For a circular cylinder, the reference area is the outer diameter, for the heave plate, the plate area is used, and for chain, the chain diameter is used.

Mooring system

In order to ensure that the mooring system in the numerical model represents the stiffness of the system correctly, the pre-tension and restoring forces of the mooring system were validated. The pre-tension was taken as the mean mooring line tension in the system at rest. It was found that the configuration given in the model test setup description gave accurate results, as shown by the pretension in Tab. 5.

TABLE 5: MOORING LINE PRETENSION.

	Experiment	Numerical model
Line no.	(kN)	(kN)
1	1675	1666
2	1680	1666
3	1649	1666

The mooring system restoring properties were validated by comparing pull-out tests from the Ocean Basin to quasi-static analysis with a slowly increasing force applied to the floater. The obtained mooring line tension and system restoring force showed good agreement with the model test results, as shown in Fig. 3. The system restoring force was taken as the applied pull-out force in the model test, and the applied force in the origin in the numerical model.

After the static properties of the mooring system were established, the dynamic behaviour was assessed by applying prescribed floater motions to a model with mooring lines only.

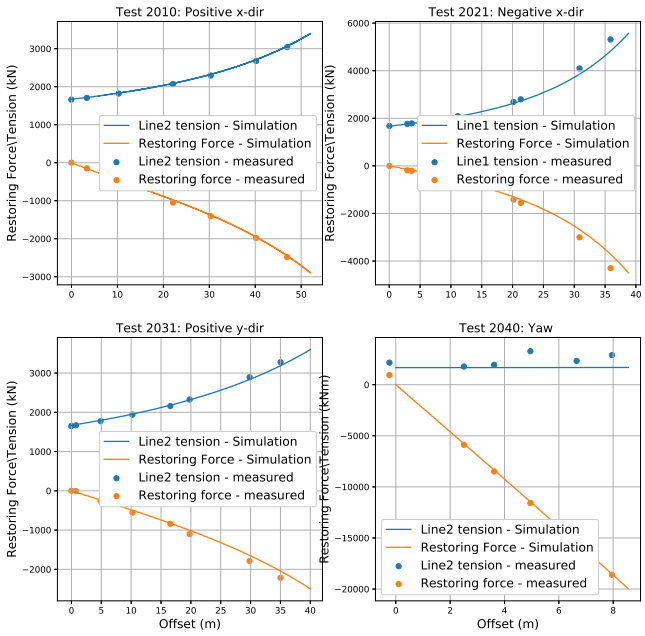

FIGURE 3: PULL-OUT TESTS. MOORING LINE TENSION AND RESTORING FORCE OF THE SYSTEM.

Floater motion and wave timeseries from irregular wave test 6250 was applied, and mooring line tensions were compared to measurements.

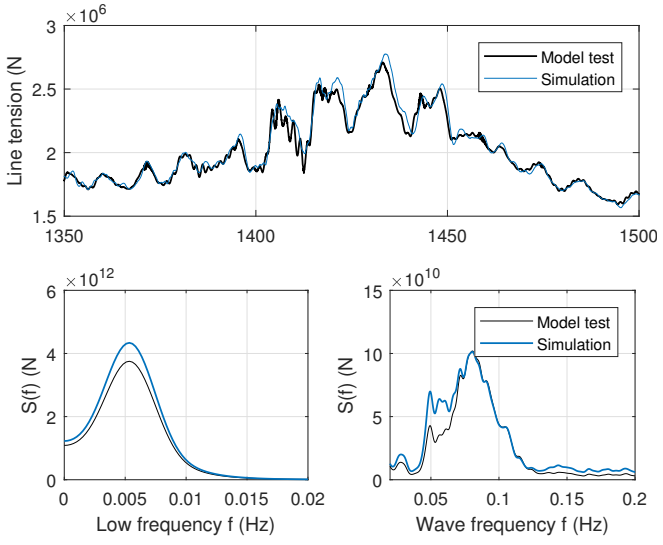

FIGURE 4: MOORING LINE TENSION.

A drag coefficient of 2.8 for the chain segments and 1.0 for the clump weight was found to give good agreement with line tension measurement in irregular waves. By comparison, the DNV GL design standard for mooring [8] specifies a coefficient of 2.4 for studless chain. Figure 4 shows a sample of the time-series and the low frequency and the wave frequency spectra for line tension in the extreme sea state test for simulations applying a drag coefficient of 2.8. A drag coefficient of 2.0 gave the best representation of the response around 0.05 Hz, but underestimated the response in the rest of the wave frequency range. High frequencies were not represented well, irrespective of drag coefficient, but the amplitude of these responses were small compared to the low- and wave frequency response. The spectrum plot horizontal axis was cut off at 0.2 Hz, as no visible contribution could be seen beyond this frequency. The resulting dynamic response of the mooring lines in extreme irregular waves are shown in Fig. 4.

It should also be mentioned that it was found necessary to include the added mass of the clump weights. An added mass of 7292 kg in lateral direction was applied to each clump weight.

Free decay

The decay tests of the moored platform in calm environment, without the ReaTHM system, were used to find the natural periods and the modal damping in the experiments. Eigenperiods and damping were compared to numerical free decay tests. The eigenperiods were taken as the average time between 6-13 peaks, depending on the response type and the length of the signal.

Good correspondence between the experiments and the numerical model was found for surge, heave, pitch and and yaw.

Table 6 lists the natural periods obtained from decay analysis of experiments and numerical analysis. The pitch natural frequency that is shown here, was obtained in the numerical analysis with the adjusted centre of gravity.

The tower fore-aft bending frequency was adjusted to match the model test by changing the stiffness of the element connecting the tower to the platform.

For each pair of consecutive peaks with average amplitude $\bar{X}$ of the decay response, the logarithmic damping decrement (δ) was found, and the damping ratio (ζ) calculated calculated by Eq. 2.

$$\zeta(\bar{X}) = \frac{1}{\sqrt{1+\left(\frac{2\pi}{(\delta(\bar{X}))^2}\right)}} \tag{2}$$

From the method of equivalent linearisation, as described in e.g. [9], the modal damping ratio for a mode with natural frequency ω_n, can be expressed as a function of oscillation amplitude X:

TABLE 6: Natural periods.

Mode	Experiment (s)	Numerical model (s)
Surge	178.3	185.2
Heave	20.5	20.7
Pitch	34.4	34.8
Yaw	95.3	99.0
Tower FA bending (free floating system)	1.71	1.71

$$\zeta(X) = \frac{B_1 + B_2 \frac{8\omega_n}{3\pi} X}{B_{cr}} \tag{3}$$

where B_1 and B_2 are the linear and quadratic damping coefficients, respectively, B_{cr} is the critical damping and m is the mass of the system.

TABLE 7: DRAG COEFFICIENTS DETERMINED FROM DECAY IN CALM WATER.

Component	Direction	Cd (-)
Column	horizontal	0.6
Pontoon	horizontal	1.3
Pontoon	vertical	5.0
Heave plates	vertical	21.0

In the damping model represented by Eq. 3, the linear damping determines the intercept of the damping ratio curve, and the quadratic damping determines the slope.

In figure 5 it can be seen that damping measured in the model test showed to vary approximately linearly with the mean amplitude of two consecutive cycles. Heave and pitch and yaw seemed to have contributions from linear damping that are less than 1%. For surge motion, the linear damping ratio (intercept) appears to be between 1.5 and 2%.

Since the measured damping had an apparent dependency on oscillation amplitude, Eq. 3 suggests that it is necessary to model

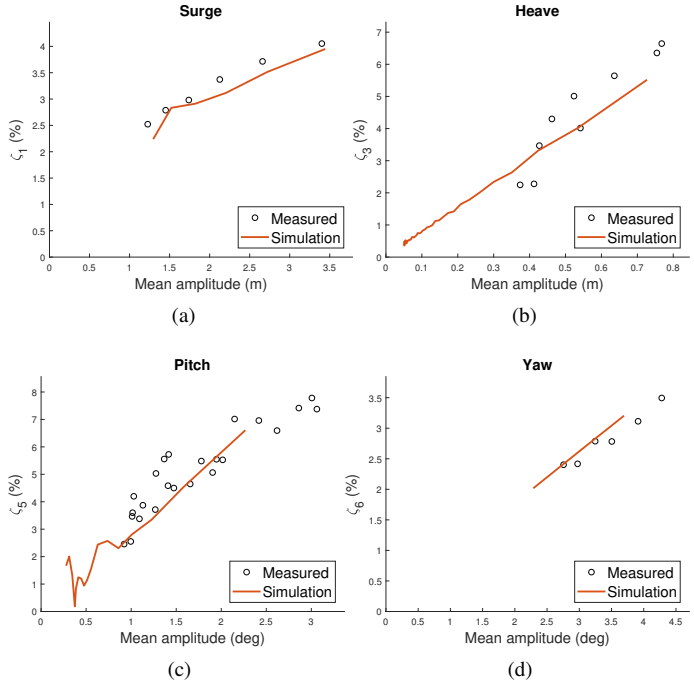

FIGURE 5: DAMPING RATIO AS A FUNCTION OF MEAN AMPLITUDE FOR EXPERIMENTS AND NUMERICAL MODEL WITH TUNED DRAG COEFFICIENTS.

quadratic damping in the simulations. Thus, the drag coefficients were adjusted to fit the damping measured in the Ocean Basin.

The pontoons had a box cross-section with 0.5 m wide girders at the keel, which will give different drag characteristics horizontally and vertically. This was modelled by applying different coefficients for drag in the vertical and horizontal directions.

Vertical drag coefficients for pontoons and heave plates were calibrated to decay tests of heave and pitch motion, and the resulting decay simulation matched the damping levels from the model tests quite well.

The horizontal drag coefficients were calibrated to match yaw and surge decay motions. It proved difficult to match both surge and yaw by quadratic drag coefficients alone, so linear damping in surge (B_{11}) and sway was added to the platform, corresponding to 1.5% of critical damping (see Eq. 4). This linear damping term came in addition to the frequency dependent linear damping obtained from the potential flow analysis.

$$B_{11} = 0.015 * 2 * (M_{11} + A_{11}) * \frac{2\pi}{T_1} \tag{4}$$

where M_{11} is the total mass of the platform, A_{11} is element (1,1) in the added mass matrix for the platform, and T_1 is the resonance

period in surge/sway.

A number of different combinations of horizontal drag coefficients for the columns and the pontoons gave good comparisons with the decay tests. A theoretical consideration of the horizontal drag coefficient for the column was made based on Reynolds-/KC-numbers in [6], and the conclusion was that 0.6 was appropriate in sea states relevant for this platform, due to high Reynolds numbers (full scale). Therefore, in the calibration, the combination including 0.6 for the columns was chosen for further comparison with model tests.

The drag coefficients resulting from the calibration exercise for decay in calm water are shown in Tab. 7. For comparison, the model scale drag coefficient of a smooth cylinder with diameter 13.4 m in the irregular wave test with H_s=10.9 m and T_p=15 s is 0.23, according to [10]. For the same cylinder moving with an amplitude of 3.5 m and a period equal to the surge period of this platform, the drag coefficient is 0.5.

Applying the coefficients in Tab. 7, the resulting damping ratio as function of mean oscillation amplitude for surge, heave, pitch and yaw are shown in Fig. 5.

In a separate exercise, the quadratic damping coefficient matrix was tuned to match the free decay experiments. This was used to show the difference between a pure potential theory model, including quadratic damping, and a model including viscous forces (see Figs. 8, 7 and 6).

Irregular wave tests

The drag term in the Morison type forces includes the relative velocity between the wave particle velocity and the velocity of the moving structure, and therefore contributes with both excitation and damping. For that reason, applying drag coefficients calibrated to decay tests in analyses with waves, can result in uncorrect response to wave loads. Thus, for application to analysis with waves, drag coefficients must be calibrated with waves present.

Contribution from the viscous terms to mean drift surge excitation of a semi-submersible can come from both the horizontal and the vertical term, as described in [11]. Horizontal terms contribute to the mean wave force above the water line, and vertical viscous terms contribute to the horizontal terms through coupling with pitch motion.

It was observed in the analysis, that surge resonant motion was insensitive to changes in the vertical drag coefficients.

Calibrating drag in irregular waves can be tricky, as increasing the coefficient will not only increase the excitation, but also the damping. Recognizing that most of the contribution to the mean wave force comes from the drag force on members near the free surface, an approach with different drag coefficients on the upper (down to 4 m below MWL) and lower parts of the columns were applied. This way it is possible to be flexible to match both the mean and varying part of the wave loads without compromising one or the other. This approach has also been successfully applied in semi-submersible simulations earlier, by Berthelsen et. al. [2, 12].

In the horizontal direction, the drag coefficients for the columns and pontoons were calibrated to match surge motion from the model test. First, a uniform coefficient for the columns was found by calibrating against the mean surge motion from the model test (see Fig. 6). Then, drag coefficients for the lower part of the columns and for the pontoons were adjusted to match the surge frequency peak in the response spectrum for surge motion (see Fig. 7). This also influenced the standard deviation and maximum value, shown in Fig. 6. The resulting coefficients calibrated after irregular wave test 6250 are listed in Tab. 8.

Timeseries for floater motions and mooring line tension, and statistics for surge motion and mooring line tension are shown in Figs. 8 and 6, respectively, for irregular wave analysis applying three different approaches;

1. potential theory with quadratic damping matrix, $C_d = 0$
2. uniform horizontal drag coefficient for the entire length of the column, as calibrated in decay tests,
3. combined approach with a coefficient tuned to match the mean surge response in irregular waves on the upper part (-4 m below MWL to wave elevation) and a smaller coefficient on the lower part, tuned to match low frequency surge response.

TABLE 8: Drag components determined from irregular wave test 6250.

Component	Direction	Cd (-)
Column upper	horizontal	0.8
Column lower	horizontal	0.35
Pontoon	horizontal	0.8
Pontoon	vertical	0.7
Heave plates	vertical	12.0

Figure 7 shows that applying potential drift forces, and a quadratic damping matrix tuned to decay tests, underestimated the low frequency response. The model excluding the quadratic damping matrix overestimated the low frequency response (not shown here).

Reducing the horizontal drag coefficient for the pontoon, had the same effect as reducing the coefficient for the lower part of the columns. This is as expected, since the total surge force

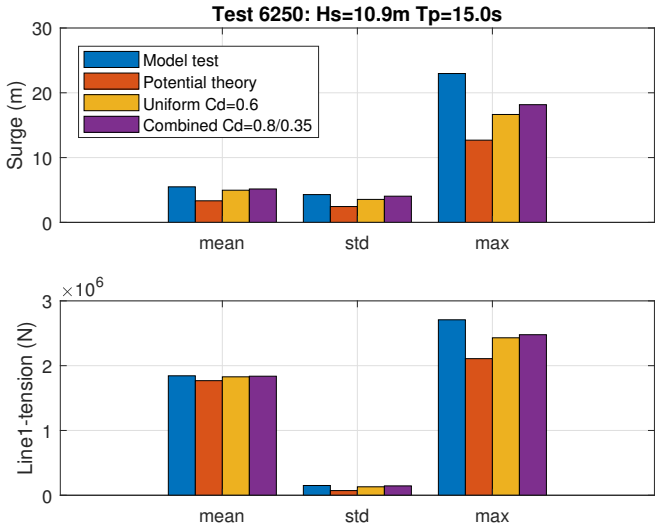

FIGURE 6: RESPONSE STATISTICS FOR IRREGULAR WAVE TEST 6250.

contains contribution from horizontal forces on all submerged members. Thus, various combinations of horizontal coefficients for columns and pontoons can yield the same low frequency response in surge. In pitch, the horizontal viscous forces contribute to the surge induced pitch motion, and are thus directly related to surge response. Thus, all combinations of horizontal coefficients that gave good correspondence for surge motion, also gave good correspondence for pitch motion. It was decided to continue with a combination where the coefficient for the box cross-section was higher than for the circular cross-section, since it can be argued that this is more physical for similar motion amplitudes and flow conditions.

As seen in Fig. 7, the numerical model with the uniform column coefficients underpredicts pitch response around the pitch natural frequency (0.029 Hz). Since this is resonant response, damping is important, and thus, an attempt was made to tune the vertical drag coefficients to match this response peaks. However, coefficients that led to more accurate pitch motion, led to less accurate heave response. Therefore, the vertical coefficients were kept at a level that did not cause higher heave excitation than the model tests. In any case, both vertical coefficients needed to be significantly reduced compared to what was obtained for the decay tests. A heave plate drag coefficient of C_d=12 was found to give good correspondence with the pitch resonance response statistics from the experiments (see Fig. 6), and this is the same value determined from the theoretical consideration made in [6].

The numerical model with the tuned coefficients gave good agreement between simulations and experiments in both the wave frequency and low frequency range. The same is true for line tension, which seemed to be closely related to surge motion. Surge induced pitch motion, as seen in Fig. 7(c), followed

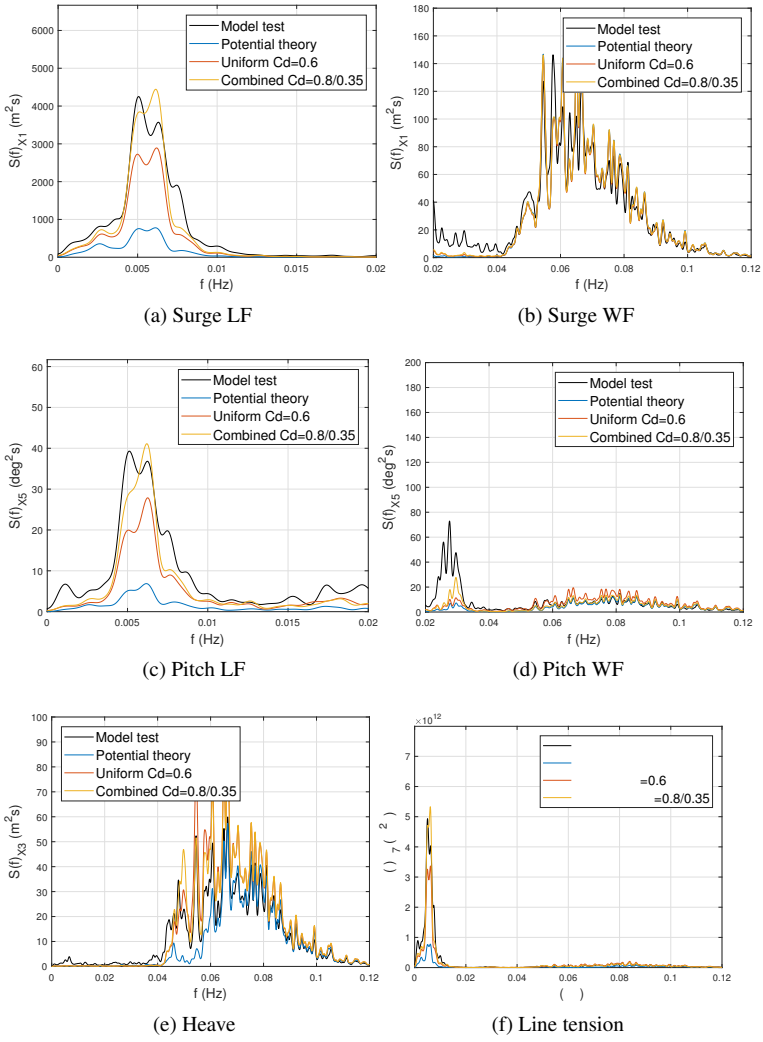

(a) Surge LF (b) Surge WF

(c) Pitch LF (d) Pitch WF

(e) Heave (f) Line tension

FIGURE 7: LOW FREQUENCY (LF) AND WAVE FREQUENCY (WF) RESPONSE SPECTRA FOR IRREGULAR WAVE TEST 6250.

the surge response closely. Pitch resonance (Fig. 7(d)) was improved by adjusting the vertical drag coefficients.

Low frequency heave response was not captured well by the numerical model (see Fig. 7(e)). However, this can not be expected since Newman's approximation is only valid for surge, sway and yaw. Also, there are no non-zero contribution to the mean vertical force from the viscous forces [11]. To capture this response, full quadratic transfer functions must be applied.

Although similar mean and standard deviations for surge response was achieved, the maximum response in the simulation was smaller than what was seen in the experiments (see Fig. 6. By studying the video of the experiments, it could be seen that the maximum surge response occurred soon after a wave over-

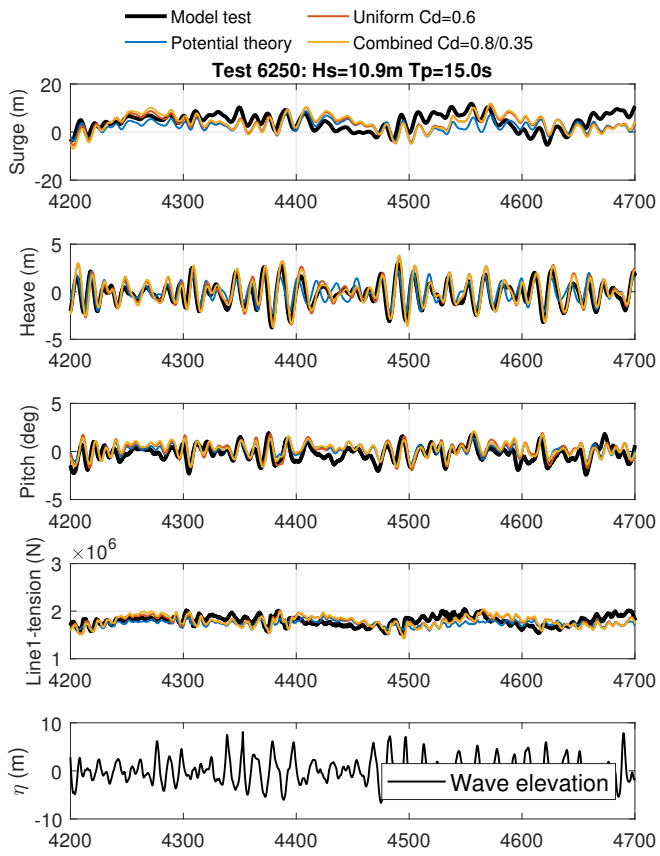

FIGURE 8: RESPONSE TIMESERIES FOR IRREGULAR WAVE TEST 6250.

topped one of the columns. This is a highly non-linear event that could not be modelled.

Irregular wave test 6250 is an extreme sea state, where the column diameter to wavelength ratio is 0.04 and wave height to column diameter ratio is 0.8. Placed in a theory validity diagram [10], this means that both inertia effects and viscous effects contribute to the wave forcing. For more moderate sea states, the wave height to column diameter ratio is lower, and drag effects become less important. The next step was to compare the calibrated numerical model to test no. 6410, representing a more moderate seastate with Hs=5.5 m and Tp=9.0 m.

Response timeseries for the more moderate seastate is shown in Fig. 10, response spectra in Fig. 9. Surge response is reasonably well predicted, both in the wave frequency and the low frequency range. The horisontal coefficients determined for the more severe seastate seem to give a good estimate also here. Looking at the heave response spectrum, however, one can see that heave resonance (0.049 Hz) is underpredicted, and almost not present in the simulation. This could be due to the lack of a second order low frequency excitation in heave in the numerical model. Pitch resonance is also underpredicted.

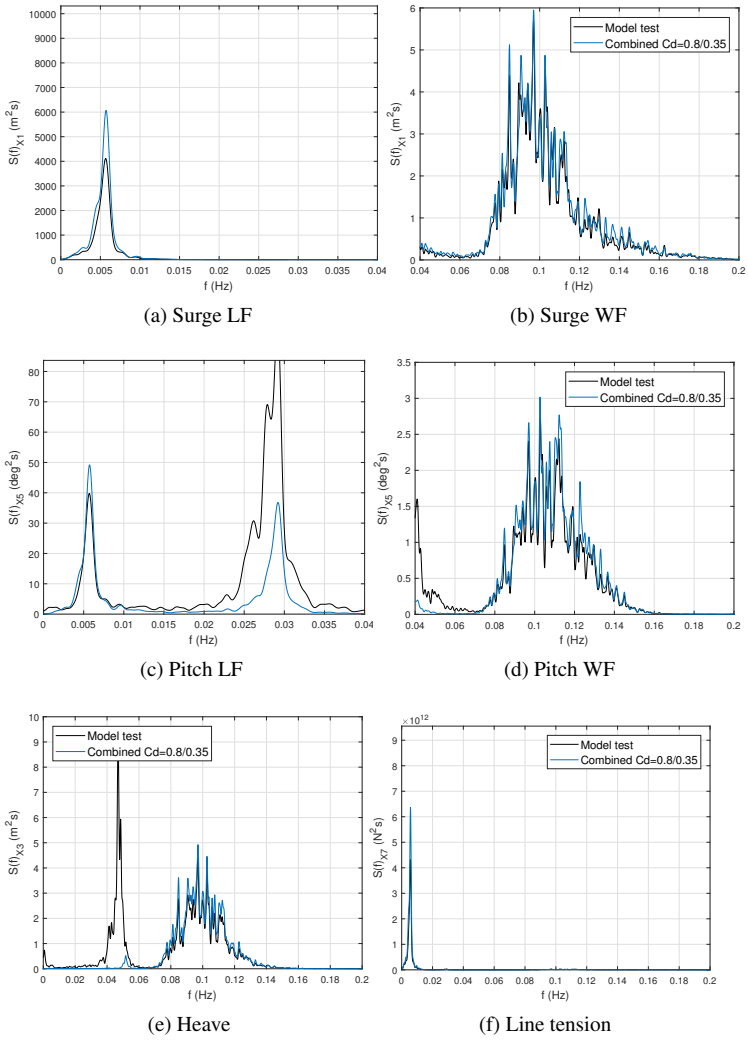

(a) Surge LF (b) Surge WF

(c) Pitch LF (d) Pitch WF

(e) Heave (f) Line tension

FIGURE 9: RESPONSE SPECTRA FOR IRREGULAR WAVE TEST 6410.

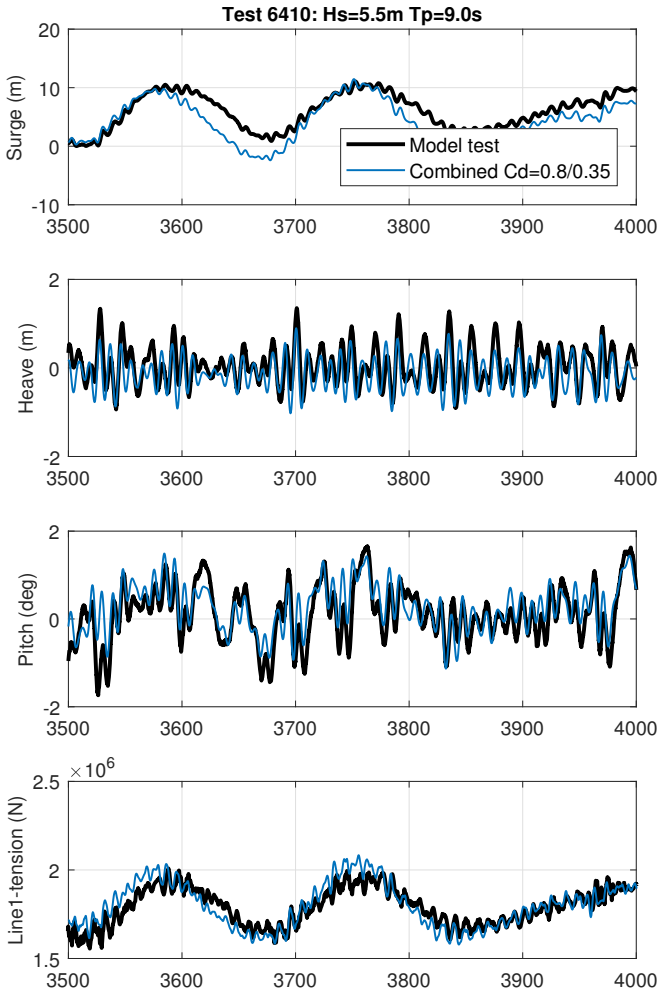

FIGURE 10: RESPONSE TIMESERIES FOR IRREGULAR WAVE TEST 6410.

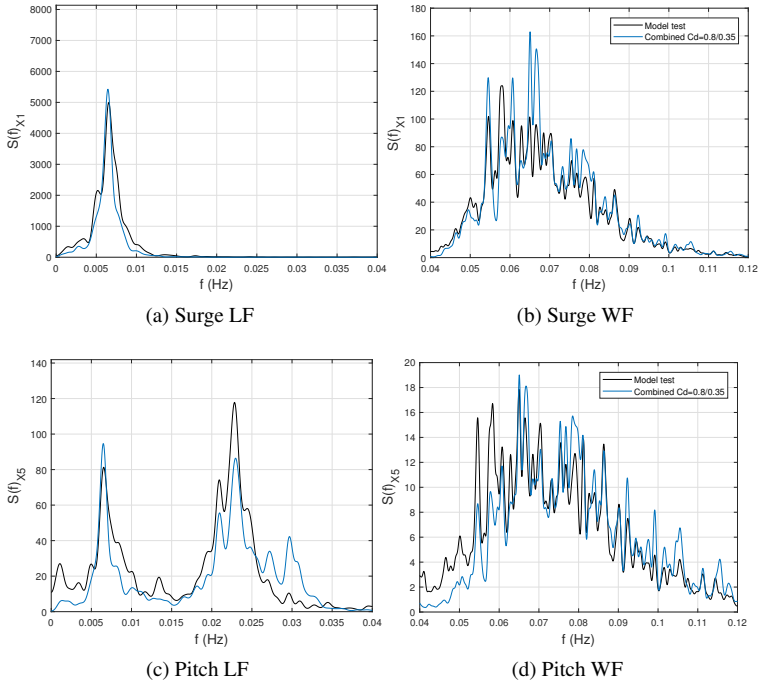

(a) Surge LF (b) Surge WF

(c) Pitch LF (d) Pitch WF

FIGURE 11: RESPONSE SPECTRA FOR IRREGULAR WAVE TEST WITH WIND (6231).

Irregular wave tests with turbulent wind

Following the calibration of drag coefficients to irregular wave tests, simulations with turbulent wind on an operating turbine were carried out. To avoid uncertainties in the modelling of the aerodynamic loads, the measured resulting wind force on the rotor was applied directly in the simulation, together with wave elevation measurements from the experiment. Test 6231 contains the same waves as the wave only test 6250, and 18 m/s mean wind speed with IEC Normal Turbulence Model.

Response timeseries for the more moderate seastate is shown in Fig. 12, response spectra in Fig. 11. Surge, pitch and heave response spectra and statistics are well predicted, both in the wave frequency and the low frequency range.

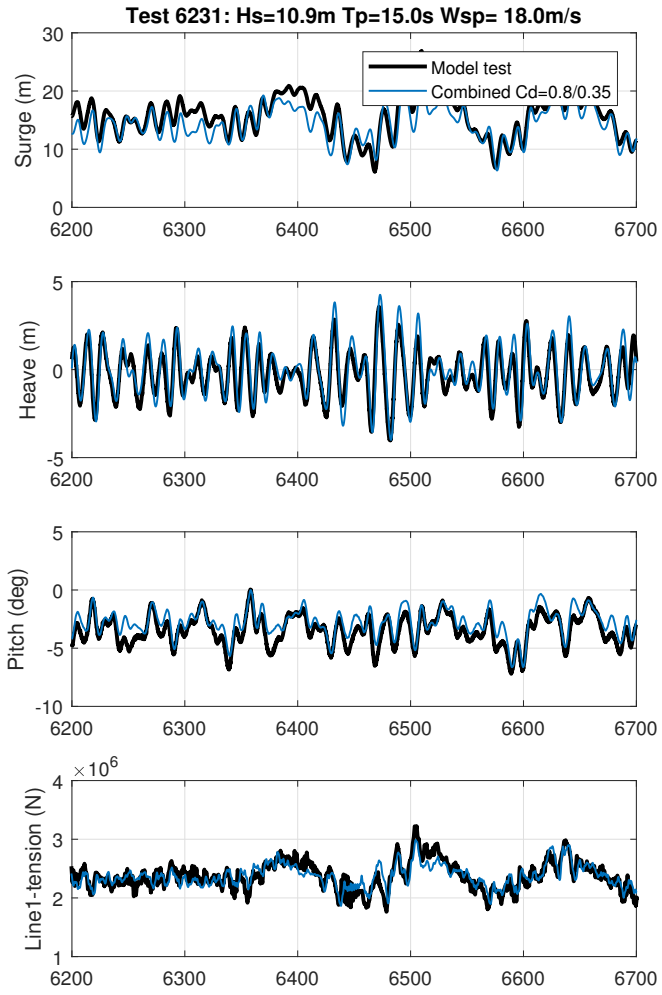

FIGURE 12: RESPONSE TIMESERIES FOR IRREGULAR WAVE TEST WITH WIND (6231).

CONCLUSIONS

Calibration of a numerical model emulating the experiments with a semi-submersible 10MW wind turbine, carried out at SINTEF Ocean in connection with the LIFEs50+ project, was described and discussed in this paper. It was found that applying potential theory wave forces, including slow drift forces by Newman's approximation and a tuned quadratic damping matrix, underestimated the low frequency surge response, and also the surge induced responses in pitch and mooring line tensions. The drag coefficients determined from decay tests led to underestimated low frequency surge motions in irregular sea states. An approach applying different horizontal drag coefficients in the wave zone and the lower part of the columns successfully adjusted the model to reproduce similar low frequency motions.

Pitch resonant response was somewhat underestimated in the simulations, but adjusting vertical drag coefficients gave a better prediction. It should be noted that other combinations of coefficients for column, pontoon and heave plates, than what is reported here can also reproduce the model test response. These combinations were always in a range around the reported coefficients.

The wave frequency response was, except for the mooring line response, relatively unaffected by the variation of drag coefficients.

It was also shown that by applying the measured wind force in the model, that the tuned model was able to predict the floater motions in combined wind and wave analyses. Further work should include performing the same exercise to more tests with wind, and also investigate the turbine performance under events that could not be modeled, e.g. overtopping events.

It was observed that the heave resonant response seen in the model tests for moderate seastates could not be reproduced by the numerical model. A model including full quadratic transfer functions should be applied to capture this response. Also, wave overtopping events were observed, closely followed by extreme response that could not be predicted by the model.

ACKNOWLEDGMENT

The research leading to these results has received partial fundings from the European Union Horizon2020 programme under the contract H2020-LCE-2014-1-640741, and partial fundings from the Research Council of Norway and EU FP7 grant agreement 609795 (IRPWIND). Also, we are grateful to Dr. techn. Olav Olsen AS for the permission and contribution to set up the public 10MW semi-submersible design based on their concept of the OO-Star Wind Floater (www.olavolsen.no).

REFERENCES

[1] Robertson, A. N., Wendt, F., Jonkman, J. M., Popko, W., Dagher, H., Gueydon, S., Qvist, J., Vittori, F., Azcona, J.and Uzunoglu, E., et al., 2017. "OC5 project phase II: validation of global loads of the deepcwind floating semisubmersible wind turbine". *Energy Procedia,* ***137***, pp. 38–57.

[2] Berthelsen, P. A., Bachynski, E. E., Karimirad, M., and Thys, M., 2016. "Real-Time Hybrid Model tests of a braceless semi-submersible wind turbine: Part IIIcalibration of a numerical model". In ASME 2016 35th International Conference on Ocean, Offshore and Arctic Engineering, American Society of Mechanical Engineers.

[3] Thys, M., Eliassen, L., Chaubaud, V., Sæther, L. O., Magnussen, Ø. B., and Sauder, T., 2018. "Real-Time Hybrid Model testing of a semi-submersible 10MW floating wind turbine, including blade elasticity and extreme design cases". In ASME 2018 37th International Conference on Ocean, Offshore and Arctic Engineering, American Society of Mechanical Engineers. Paper no. OMAE2018-78131.

[4] Sauder, T., Chabaud, V., Thys, M., Bachynski, E. E., and Sæther, L. O., 2016. "Real-Time Hybrid Model testing of a braceless semi-submersible wind turbine: Part Ithe hybrid approach". In ASME 2016 35th International Conference on Ocean, Offshore and Arctic Engineering, American Society of Mechanical Engineers.

[5] Bachynski, E. E., Thys, M., Sauder, T., Chabaud, V., and Sæther, L. O., 2016. "Real-Time Hybrid Model testing of a braceless semi-submersible wind turbine. part II: Experimental results". In 35th International Conference on Ocean, Offshore and Arctic Engineering, no OMAE2016-54437.

[6] Yu, W., Müller, K., Lemmer, F., Schlipf, D., Bredmose, H., Borg, M., Landbø, T., and H., A., 2017. LIFEs 50+: Deliverable D4.2 Public Definition of the Two LIFES50+ 10MW Floater Concepts. Tech. rep., July.

[7] Bak, C., Zahle, F., Bitsche, R., Kim, T., Yde, A., Henriksen, L. C., Hansen, M., Blasques, J., Gaunaa, M., and Natarajan, A., 2013. Description of the dtu 10 MW reference wind turbine. DTU wind energy report-I-0092. Tech. rep.

[8] DNV GL, DNVGL-OS-E301, 2015. *DNVGL-OS-E301, Position mooring*.

[9] Langen, I., and Sigbjörnsson, R., 1979. *Dynamisk analyse av konstruksjoner: Dynamic analysis of structures*. Tapir.

[10] DNV GL, DNVGL-RP-C205, 2017. *DNVGL-RP-C205, Environmental conditions and environmental loads*.

[11] Faltinsen, O. M., 1990. *Sea Loads on Ships and Ocean Structures*. Cambridge University Press.

[12] Berthelsen, P. A., Baarholm, R., Pákozdi, C., Stansberg, C. T., Hassan, A., Downie, M., and Incecik, A., 2009. "Viscous drift forces and responses on a semisubmersible platform in high waves". In ASME 2009 28th International Conference on Ocean, Offshore and Arctic Engineering, American Society of Mechanical Engineers, pp. 469–478.